Elliptic flow of thermal photons from an event-by-event hydrodynamic model

Rupa Chatterjee,[1,2,*] Hannu Holopainen,[3,†] Ilkka Helenius,[1,4,‡] Thorsten Renk,[1,4,§] and Kari J. Eskola[1,4,‖]

[1]*Department of Physics, P.O. Box 35, FI-40014 University of Jyväskylä, Finland*
[2]*Variable Energy Cyclotron Centre, 1/AF, Bidhan Nagar, Kolkata-700064, India*
[3]*Frankfurt Institute for Advanced Studies, Ruth-Moufang-Str. 1, D-60438 Frankfurt am Main, Germany*
[4]*Helsinki Institute of Physics, P.O. Box 64, FI-00014 University of Helsinki, Finland*

Elliptic flow of direct photons in relativistic heavy ion collisions is believed to be dominated by contribution from thermal radiation of quark gluon plasma up to $p_T \sim 5$ GeV/c, although other sources start outshining the thermal contribution at already smaller values of p_T in the direct photon spectrum. The elliptic flow of thermal photons from ideal hydrodynamics considering a smooth initial density distribution underpredicts the PHENIX direct photon data from 200A GeV Au + Au collisions at the Relativistic Heavy Ion Collider (RHIC) by a large margin in the range $1 < p_T < 5$ GeV/c. However, a significant enhancement of thermal photon production due to fluctuations in the initial QCD matter density distributions is expected. We show that such fluctuations result in substantially larger photon elliptic flow for $p_T > 2.5$ GeV/c compared to a smooth initial-state-averaged density profile. The results from event-by-event hydrodynamics are found to be sensitive to the fluctuation size parameter. However, the effects of initial state fluctuations are insufficient to account for the discrepancy to the PHENIX data for direct photon elliptic flow. Furthermore, the photon v_2 is reduced even more when we include the NLO pQCD prompt photon component. We also calculate the spectra and elliptic flow of thermal photons for 2.76A TeV Pb + Pb collisions at the Large Hadron Collider (LHC) and for the 0–40% centrality bin. Thermal photons from event-by-event hydrodynamics along with prompt photons from NLO pQCD calculations explain the ALICE preliminary direct photon data well in the region $p_T \geqslant 2.5$ GeV/c. Similar to RHIC, the elliptic flow results at LHC are again found to be much smaller than the ALICE preliminary v_2 data.

I. INTRODUCTION

Recent fluid-dynamics simulations have shown that event-by-event (E-by-E) fluctuating initial conditions (IC) are more realistic than smooth initial density distributions to model the evolution of the hot and dense matter produced in relativistic heavy ion collisions [1–4]. Hydrodynamics with fluctuating IC reproduces the experimental charged particle elliptic flow even for the most central collisions at the Relativistic Heavy Ion Collider (RHIC) [1] which was underestimated by all earlier hydrodynamic calculations using smooth IC. E-by-E hydrodynamics also gives a better agreement of the experimental charged particle spectra towards higher p_T by hardening the spectra [1,5], helps to understand the various structures observed in two-particle correlations [6] and is a necessary element in determining the shear viscosity (η/s) from simultaneous measurements of elliptic and triangular flow coefficients [7].

Thermal emission of photons is known to be sensitive to the initial temperature of the system where photons with large transverse momentum are emitted mostly from the hot and dense early stage of the system [8]. Thus, they can be considered as one of the most promising probes to study fluctuations in the initial density distributions. In recent studies we have shown that E-by-E hydrodynamics with fluctuating IC enhances the production of thermal photons significantly in the region $p_T > 1$ GeV/c compared to a smooth initial-state-averaged profile in an ideal hydrodynamic calculation [9]. This enhancement is mostly an early time effect when the radial flow is small and the 'hotspots' in the fluctuating IC produce more high p_T photons than the smooth IC. The relative importance of IC fluctuations is found to increase for peripheral collisions and for lower beam energies [10].

For a noncentral collision of two spherical nuclei the overlapping zone between the nuclei no longer remains circular but it rather takes an almond shape. This initial spatial anisotropy of the overlapping zone is converted into momentum space anisotropy of particle distribution via the action of azimuthally anisotropic pressure gradients. The anisotropy is quantified by decomposing the invariant particle distribution in the transverse momentum plane in Fourier series as

$$\frac{dN}{d^2 p_T dY} = \frac{1}{2\pi} \frac{dN}{p_T dp_T dY} \left[1 + 2 \sum_{n=1}^{\infty} v_n(p_T) \cos(n\phi) \right],$$
(1)

where ϕ is the azimuthal angle measured with respect to the reaction plane. The most important term in the equation above is v_2, elliptic flow, which is related to the almond shape mentioned above. Elliptic flow has been one of the key observables studied at the RHIC experiments [11], where large v_2 values are considered as a sign of collectivity in the produced system.

————————
*rupa@vecc.gov.in
†holopainen@fias.uni-frankfurt.de
‡ilkka.helenius@jyu.fi
§thorsten.renk@phys.jyu.fi
‖kari.eskola@phys.jyu.fi

The elliptic flow of thermal photons shows interesting behavior as a function of p_T due to the interplay of the contributions from quark matter and hadronic matter phases which dominate the flow results at different stages of the system evolution [12,13]. The low p_T part of the thermal photon elliptic flow is dominated by the contribution from the hadronic phase whereas the high p_T part represents photons emitted from the QGP phase at the beginning of the system expansion having small transverse and elliptic flow. As a result the thermal photon v_2 from hydrodynamics is very small at large p_T ($\sim$5 GeV/c), where the emission is dominated by the QGP phase. Elliptic flow rises with decreasing p_T and then falls again when p_T is decreased further and the maximum is around 1.5–2.5 GeV/c [12].

It has been shown that the contributions from different sources of direct photons (apart from thermal) become significant in the photon p_T spectrum for $p_T > 3$ GeV/c [14]. However, the thermal radiation dominates the elliptic flow of direct photons up to a much larger p_T ($\sim$5 GeV/c) as the v_2 contributions from other sources are marginal in that range [14]. Prompt photons produced in primary interactions do not exhibit any azimuthal anisotropy and their contribution to the flow coefficient v_2 is zero. Photons from fragmentation and jet conversion have a very small positive and negative elliptic flow respectively, which tend to cancel each other [14]. Thus, the only contribution that survives in the low and intermediate p_T range is the azimuthal anisotropy of thermal photons. Thermal photon elliptic flow using $(3 + 1)$-dimensional hydrodynamics [15] has also been found to be quite similar to the results obtained with a $(2 + 1)$-dimensional calculation [12].

The PHENIX Collaboration has measured a large elliptic flow of direct photons for $200A$ GeV Au + Au collisions at RHIC [16]. The photon v_2 data shows similar qualitative behavior as predicted by hydrodynamic calculations using smooth IC and optical Glauber model. However quantitatively, the results from the theory calculations [12–14] underpredict the data by a large margin. Similar results have also been observed at the Large Hadron Collider (LHC) energy [17].

In this paper we study the effect of initial state fluctuations on the elliptic flow results of thermal photons and discuss the large difference between the experimental data and results from E-by-E hydrodynamics. For recent similar investigations, discussing also viscous effects, see Ref. [18].

II. EVENT-BY-EVENT HYDRODYNAMICS AND DIRECT PHOTONS

A. E-by-E hydrodynamics framework

We use the E-by-E hydrodynamical framework developed in [1] to model the space-time evolution of the QCD matter. This model has been successfully used to calculate the spectra and elliptic flow of hadrons with fluctuating IC [1] as well as thermal photon spectra at RHIC and LHC energies [9,10]. For simplicity this ideal hydrodynamical model assumes longitudinal boost invariance and the remaining $(2 + 1)$-dimensional problem is solved numerically with the SHASTA algorithm [19,20]. In addition, we use the equation of state (EoS) from [21] to close the set of equations.

To set up the initial distributions in a Monte Carlo Glauber (MCG) model the standard two-parameter Woods-Saxon nuclear density profile is used to randomly distribute the nucleons into the colliding nuclei. Collisions between nucleons from different nuclei take place if the transverse distance d fulfils the criterion $d^2 < \sigma_{NN}/\pi$ where we take the inelastic nucleon-nucleon cross section $\sigma_{NN} = 42$ and 64 mb for RHIC and LHC, respectively.

The hydrodynamical calculation is initialized by distributing entropy density around the wounded nucleons (sWN profile). We use a two-dimensional Gaussian for smearing so that the initial entropy density is

$$s(x, y) = \frac{K}{2\pi\sigma^2} \sum_{i=1}^{N_{\mathrm{WN}}} \exp\left(-\frac{(x - x_i)^2 + (y - y_i)^2}{2\sigma^2}\right), \qquad (2)$$

where x_i, y_i are the transverse coordinates of a wounded nucleon i. K is an overall normalization constant used to fix the total amount of entropy and σ is a free parameter that controls the size of the density fluctuations. We use a value $\sigma = 0.4$ fm as default [1], but in order to understand better the effects from initial state fluctuations we vary the size parameter between 0.4 and 1.0 fm. Extending studies to even smaller values of size parameter would be interesting, but reliable calculations become numerically expensive. Since with the sWN profile the final multiplicity (entropy) grows monotonically as a function of wounded nucleons, it is meaningful to define centrality classes using fixed wounded nucleon ranges like was done in [1,10].

The initial time for the hydrodynamical calculation is taken as in [10] to be $\tau_0 = 0.17 (0.14)$ fm/c for RHIC (LHC) motivated by EKRT minijet saturation model [1,22].[1] The corresponding entropy normalization constants are $K = 102$ fm^{-1} for RHIC and $K = 250$ fm^{-1} for LHC. Freeze-out is assumed to happen on a constant temperature surface with $T_f = 160$ MeV. These choices nicely reproduce the measured p_T-spectra for positively charged pions at RHIC [1] and LHC.

B. Thermal photon emission

The quark-gluon Compton scattering and quark-anti-quark annihilation are the leading order processes for thermal photon production in the partonic phase. Also the bremsstrahlung processes, which need to be taken into account in the full leading order calculation, contribute significantly to the production [24]. It has been shown in a very recent study that the inclusion of next-to-leading order (NLO) correction increases the production rate by about 20% [25] compared to the leading order result.

In the hadronic phase π and ρ mesons contribute dominantly to the photon production due to the low mass of pions and the large spin isospin degeneracy of ρ mesons [26]. The leading photon producing channels involving π and ρ mesons are $\pi\pi \rightarrow \rho\gamma$, $\pi\rho \rightarrow \pi\gamma$, and $\rho \rightarrow \pi\pi\gamma$.

As in earlier studies [9,10] we use the plasma rates $R = E dN/d^3 p d^4 x$ from [24] and hadronic rates from [27] (which

---

[1]For NLO pQCD systematics of τ_0, see Ref. [23].

at present can be considered as the state of the art) to calculate the spectra and elliptic flow of thermal photons from E-by-E hydrodynamics. The transition from the plasma rates to the hadronic rates is assumed to happen instantaneously at a temperature of 170 MeV.

The total thermal emission from the quark and the hadronic matter phases is obtained by integrating the rate equations over the space-time evolution of the medium,

$$E \, dN/d^3p = \int d^4x \, R(E^*(x), T(x)), \tag{3}$$

where $E^*(x) = p^\mu u_\mu(x)$. The four-momentum of the photon is $p^\mu = (p_T \cosh Y, p_T \cos\phi, p_T \sin\phi, p_T \sinh Y)$, and the four-velocity of the flow field is $u^\mu = \gamma_T(\cosh\eta, v_x, v_y, \sinh\eta)$ with $\gamma_T = (1-v_T^2)^{-1/2}$, $v_T^2 = v_x^2 + v_y^2$. The volume element is $d^4x = \tau \, d\tau \, dx \, dy \, d\eta$, where $\tau = (t^2 - z^2)^{1/2}$ is the longitudinal proper time and $\eta = \tanh^{-1}(z/t)$ is the space-time rapidity. The photon momentum is parametrized by its rapidity Y, transverse momentum p_T, and azimuthal emission angle ϕ.

C. Prompt photons

We know that at sufficiently high p_T the direct photon spectrum is dominated by the prompt photons originated from initial hard scatterings [14,28]. Experimentally it is not possible to separate the prompt and the thermal contributions from the direct photon spectrum. Since uncertainty arguments imply that they do not feel any medium, prompt photons are emitted isotropically and their contribution to the elliptic flow vanishes. However, their presence in the direct photon spectrum will 'wash out' the elliptic flow of thermal photons in the high-p_T region. In order to compare the experimental data for direct photon v_2 with the elliptic flow results from theory calculation, it is important to include the prompt contribution in the direct photon spectrum.

We calculate the prompt photon (direct + fragmentation) spectra in the collinear factorization framework at NLO accuracy in perturbative QCD (pQCD) using the INCNLO package [29,30]. For the parton distribution functions (PDFs) we use CTEQ6.6M set [31] with EPS09s nuclear modifications [32]. The improvement in the EPS09s nuclear PDFs (nPDFs) is that due to the inclusion of impact parameter dependence, the cross sections can be calculated in different centrality classes consistently with the globally analyzed nPDFs. For the prompt photons we determine the centrality classes in terms of impact parameter intervals, which we calculate using the optical Glauber model (see [32] for detail). The parton fragmentation to photons is calculated with BFG (set II) fragmentation functions (FFs) [33] and the fragmentation process is assumed to be unmodified with respect to the vacuum fragmentation. This assumption is not expected to hold for $A + A$ collisions in general but as the data for high-p_T direct photon R_{AA} is well reproduced with the unmodified FFs at RHIC and LHC [34–36], the assumption is reasonable. All the relevant scales (renormalization, factorization, and fragmentation) are fixed to be equal to the photon p_T.

We checked using YaJEM (which is a Monte Carlo code for in-medium shower evolution) [37] that the medium modification enhances the fragmentation photon yield by about 25 % compared to the result from vacuum calculation. This in-medium modification of the fragmentation contribution does not affect the direct photon spectrum significantly as it modifies the spectrum mostly in the region $p_T < 3$ GeV/c (shown later in upper panel of Fig. 8) where thermal radiation dominates the spectrum.

D. Elliptic flow of thermal photons

When considering smooth initial states, the available reference plane for elliptic flow calculation will always be the reaction plane (RP), which is defined by the impact parameter and beam direction. However, in the experiments the impact parameter cannot be defined. Instead in the experiments the reference plane, often called event plane, is usually defined from the final state particles in such a way that it maximizes the flow coefficient v_2.

In our case we calculate the elliptic flow with respect to the reaction plane and in E-by-E case also with respect to participant plane (PP) (which is considered a good approximation for the event plane [1]) using the relation

$$v_2^\gamma\{PP\} = \langle \cos(2(\phi - \psi_{PP})) \rangle_{\text{events}}. \tag{4}$$

The participant plane angle is defined as

$$\psi_{PP} = \arctan \frac{-2\sigma_{xy}}{\sigma_y^2 - \sigma_x^2 + \sqrt{\left(\sigma_y^2 - \sigma_x^2\right)^2 + 4\sigma_{xy}^2}}, \tag{5}$$

where

$$\sigma_y^2 = \langle y^2 \rangle - \langle y \rangle^2, \quad \sigma_x^2 = \langle x^2 \rangle - \langle x \rangle^2,$$
$$\sigma_{xy} = \langle xy \rangle - \langle x \rangle \langle y \rangle.$$

The averaging is done over the energy density in the above equations.

III. RESULTS

A. Result from a single event with changing σ values

Thermal photons are emitted from different stages of the expanding system and thus in order to gain a better understanding it is useful to study the time evolution of parameters like spatial anisotropy

$$\epsilon_x = \frac{\int dx\,dy\, \varepsilon(x, y)(y^2 - x^2)}{\int dx\,dy\, \varepsilon(x, y)(y^2 + x^2)}, \tag{6}$$

momentum anisotropy

$$\epsilon_p = \frac{\int dx\,dy\, (T^{xx} - T^{yy})}{\int dx\,dy\, (T^{xx} + T^{yy})}, \tag{7}$$

and average transverse flow velocity

$$\langle v_T \rangle = \frac{\int dx\,dy\, \varepsilon(x, y)\gamma_T v_T}{\int dx\,dy\, \varepsilon(x, y)\gamma_T} \tag{8}$$
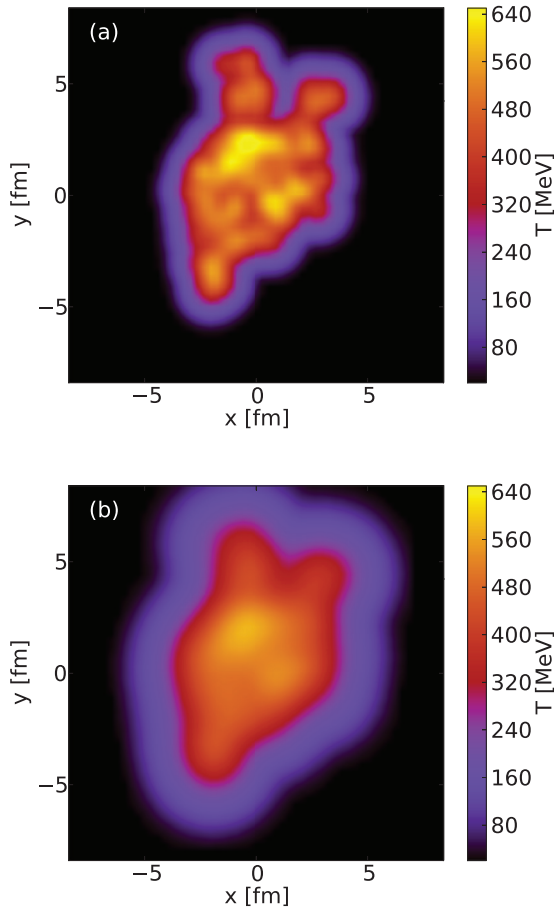
FIG. 1. (Color online) Distributions of temperature in the transverse plane at time $\tau_0 = 0.17$ fm/c for (a) $\sigma = 0.4$ and (b) $\sigma = 0.8$ fm and for $200A$ GeV Au + Au collisions at RHIC.
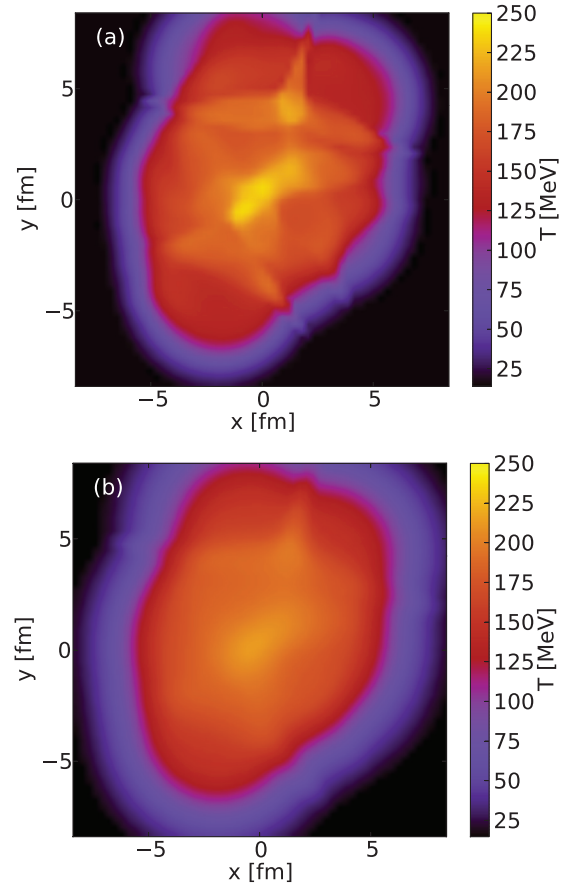

FIG. 2. (Color online) Distributions of temperature in the transverse plane at time 3 fm/c for (a) $\sigma = 0.4$ and (b) $\sigma = 0.8$ fm and for $200A$ GeV Au + Au collisions at RHIC.

from the fluctuating and smooth IC before we calculate the elliptic flow. Fluctuations in the initial density profile can make the events in the same centrality bin behave differently and thus it is difficult to compare a single event with a smooth initial state averaged profile. However, the initial states are smoother when we use a larger value for the size parameter σ. Thus, we choose an event from the fluctuating IC and change the value of σ in that particular event from 0.4 fm to 1.0 fm (in steps of 0.2 fm) and calculate the time evolution of transverse flow and anisotropy parameters to see how they are affected by the smoothness of the IC.

Figures 1 and 2 show the temperature distributions in the transverse plane at τ values 0.17 fm/c and 3.0 fm/c, respectively, for a single event from 20–40% central $200A$ GeV Au + Au collisions at RHIC. The corresponding values of impact parameter, N_{part} and N_{coll} for this particular event are 8.02 fm, 126 and 320, respectively, and they are close to the $\langle b \rangle$, $\langle N_{part} \rangle$ and $\langle N_{coll} \rangle$ for 20–40% central Au + Au collisions at RHIC. The upper panels of both the figures are for $\sigma = 0.4$ fm and the lower panels are for $\sigma = 0.8$ fm. As expected, the hotspots are more prominent for $\sigma = 0.4$ fm. These hotspots in the initial profile at $\sigma = 0.4$ fm produce more high p_T photons than the initial state averaged profile and make the spectra harder than the smoother profile [9]. Hydrodynamical

evolution further smoothes the density distribution, however the presence of hotspots can still be seen at $\tau = 3$ fm/c for $\sigma = 0.4$ fm.

The time evolution of the spatial and momentum anisotropies are shown in Fig. 3 for different values of σ. The momentum anisotropy is initially zero because there is no flow. During the evolution the pressure gradients translate the spatial anisotropy to momentum space anisotropy. Thus ϵ_x decreases and ϵ_p increases during the evolution. At time τ_0, ϵ_x is about 15% larger with $\sigma = 0.4$ fm than with 1.0 fm. From the lower panel we can see that the transverse flow develops faster with $\sigma = 0.4$ fm than 1.0 fm because pressure gradients in the system are larger with smaller values of the size parameter. For ϵ_p the early time behavior is not so clear, because looking carefully at Fig. 3 one observes that $\sigma = 0.4$ fm is not the largest scenario at early times for this particular event. From the upper panel one sees that ϵ_x falls more rapidly with time for smaller values of σ. Around 6.5 fm/c, the small and larger σ curves intersect and at larger times the order of the curves is opposite to the initial case. One also sees that ϵ_p rises rapidly with time up to 2.5–3 fm/c and then saturates as the spatial eccentricity becomes small with larger τ.

Figure 4 shows the elliptic flow of thermal photons calculated with respect to the participant plane for the same
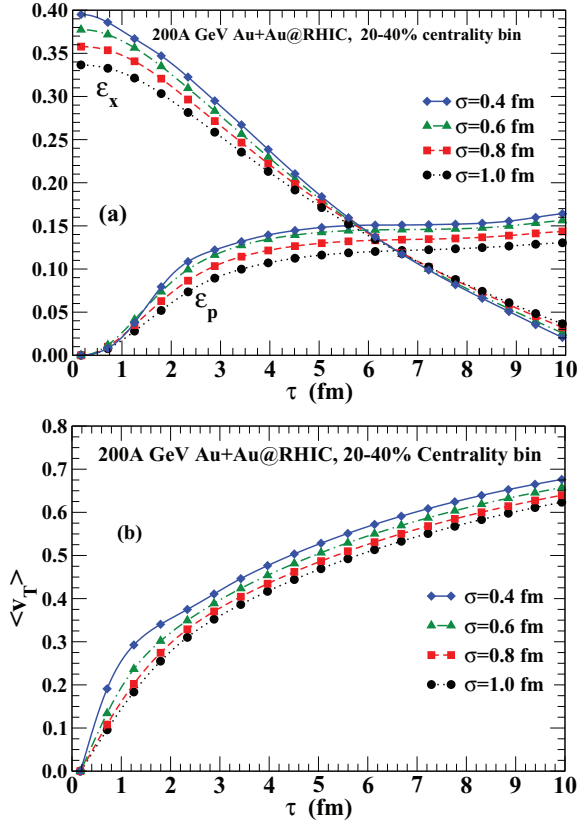
FIG. 3. (Color online) Time evolution of spatial and momentum anisotropies (a) and transverse flow velocity (b) for different values of size parameter σ for $200A$ GeV Au + Au collisions at RHIC and for 20–40% centrality bin.

FIG. 5. (Color online) The ratios of the emitted thermal photon yield as a function of time in a single event with different size parameters.

event as used in Fig. 3 and with different σ values. Since the momentum anisotropy is generally largest for the smallest size parameter, it is not surprising that the elliptic flow is largest for the smallest σ. However, at high p_T the differences between the considered cases are larger and cannot be explained by looking at the momentum anisotropy alone.

To understand better the increase in v_2 with smaller size parameter, we study the emitted photon yield as a function

FIG. 4. (Color online) Elliptic flow of thermal photons for a single event calculated with respect to the participant plane for $200A$ GeV Au + Au collisions at RHIC and for different values of σ.
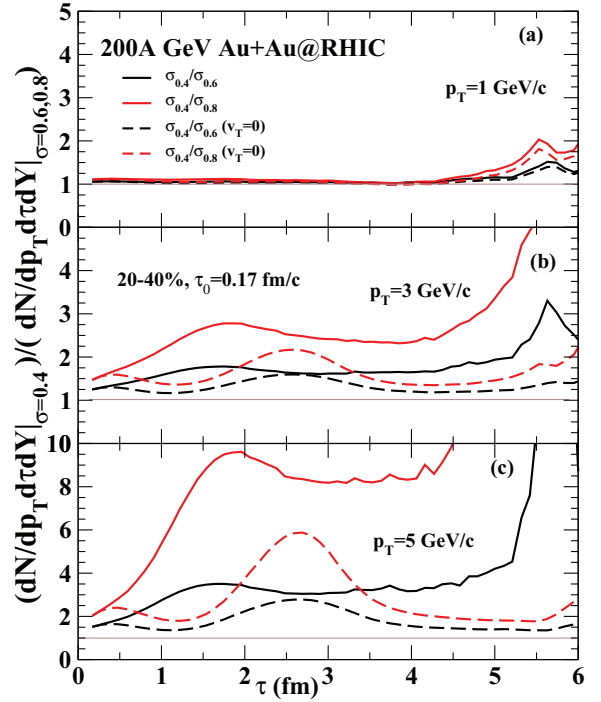
of time. Since we are interested in elliptic flow, it is more meaningful to plot the ratios of emitted yields instead of the absolute yields. These ratios are plotted in Fig. 5. The yield ratio between σ values 0.4 and 0.8 fm is larger than the ratio between σ values 0.4 and 0.6 fm. In addition we see that the ratio is smallest when τ is very small. This means that on average the emission happens later with smallest fluctuation size parameter.

We calculate the average emission time $\langle \tau \rangle$ at different σ and p_T values in order to understand this delay. With $\sigma = 0.4$ fm we get $\langle \tau \rangle = 0.6 \, \text{fm}/c$ and with $\sigma = 1.0$ fm we get $\langle \tau \rangle = 0.3 \, \text{fm}/c$ for $p_T = 5$ GeV/c. The increase in average emission time might seem too small to explain the huge difference in v_2, but for example the momentum anisotropy is an order of magnitude larger at $\tau = 0.6 \, \text{fm}/c$ than at $\tau = 0.3 \, \text{fm}/c$. As expected, the effect is most prominent for high p_T, and for example at $p_T = 1$ GeV/c the average emission time does not change as a function of σ.

The reason for the delay in the average emission time can be due to the increased transverse flow or due the existence of hot spots. The importance of these mechanisms is studied by calculating the ratio of emitted yields as a function of τ keeping $v_T = 0$ in Eq. (3) (but leaving the hydro-evolution unaltered). The results are interesting as shown by the dashed lines in Fig. 5. At very early times ($\tau \leqslant 0.5 \, \text{fm}/c$) the effect of hotspots is most pronounced as the yield ratio with $v_T = 0$ is similar to the yield ratio with non-zero v_T at all p_T and σ values. For $\tau > 0.5 \, \text{fm}/c$, transverse flow starts dominating the emission although a significant contribution from the hotspots is observed during the time period $1.5 \leqslant \tau \leqslant 3.5 \, \text{fm}/c$.
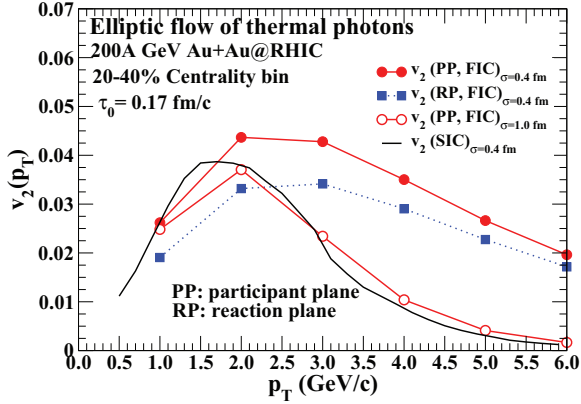
FIG. 6. (Color online) Elliptic flow of thermal photons for 200A GeV Au + Au collisions at RHIC from fluctuating and smooth IC for $\sigma = 0.4$ fm. The $v_2(p_T)$ calculated with respect to the participant and reaction planes for $\sigma = 0.4$ fm are shown by solid and dashed lines (closed symbols), respectively. v_2(PP) at $\sigma = 1$ fm is shown (solid line with open symbols) for comparison.

B. Elliptic flow from final state average at RHIC

Figure 6 shows the elliptic flow of thermal photons from fluctuating (FIC) and from smooth (SIC) initial-state-averaged IC for 200A GeV Au + Au collisions at RHIC with $\sigma = 0.4$ and 1.0 fm. The elliptic flow of thermal photons from the fluctuating IC is obtained by averaging over 200 random events and the smooth initial density distribution is obtained by taking an average of 10 000 fluctuating initial states [9]. Since in the smooth case elliptic flow is calculated with respect to the reaction plane, in order to make a fair comparison we compare it with reaction plane elliptic flow, v_2(RP), from fluctuating case. With $\sigma = 0.4$ fm the E-by-E calculation gives significantly larger elliptic flow for $p_T > 2.5$ GeV/c and for example at $p_T = 4$ GeV/c, the v_2(RP) is about 3 times larger than the result from smooth IC and the difference increases for larger values of p_T. However, with $\sigma = 1.0$ fm the increase in v_2 disappears. This behavior was expected based on our studies above with one single event.

Elliptic flow calculated with respect to the participant plane [v_2(PP)] is even larger than the reaction plane v_2 in the entire p_T range shown in the figure. This behavior is similar to the hadronic case [1] and this happens because the initial eccentricity is larger for the participant plane compared to the reaction plane. However, the difference between these two reference planes seems to have some p_T dependence and a detailed investigation is required to understand this better.

We compare our results for thermal photon elliptic flow from the fluctuating IC with PHENIX data [16] in Fig. 7. We see that the PHENIX data lie well above the results from our hydrodynamic calculations. Fluctuations clearly bring the theory towards experiment above $p_T = 2.5$ GeV/c, but still below $p_T = 4$ GeV/c the measured values are larger than our calculation. Here, in discussing the thermal photons only, we have neglected all other sources of direct photons which will make the total photon v_2 from theory calculation even smaller [13].
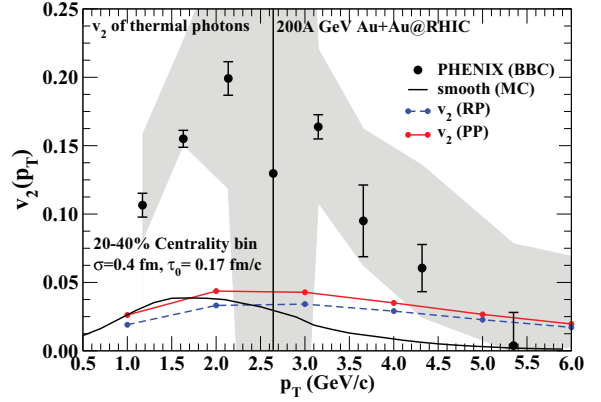

FIG. 7. (Color online) Thermal photon p_T spectra for 200A GeV Au + Au collisions at RHIC from fluctuating and smooth IC and comparison with PHENIX experimental data [16].

C. Inclusion of prompt photons

As discussed earlier, the presence of prompt photons in the direct photon spectrum decreases the elliptic flow. The corrected spectra and elliptic flow taking also the prompt photons into account are shown in Fig. 8. The PHENIX direct
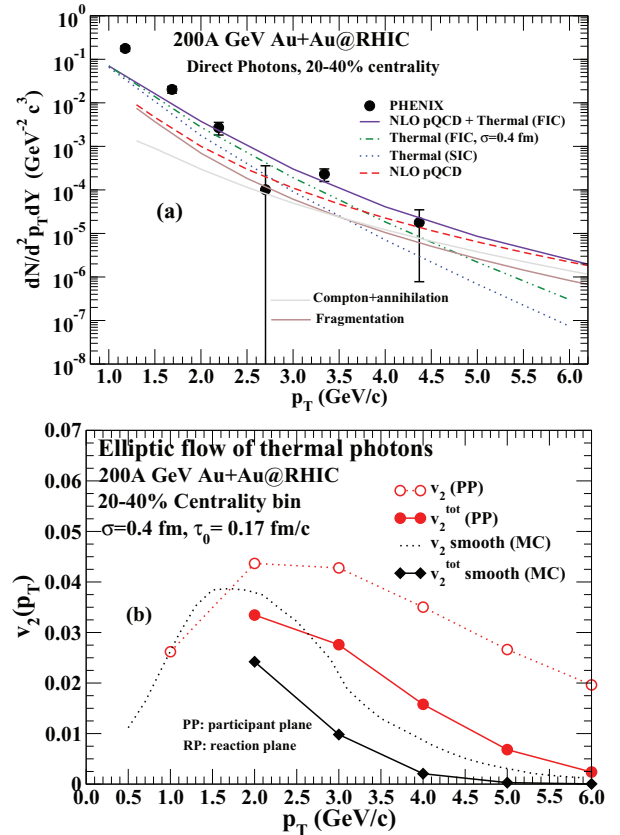

FIG. 8. (Color online) (a) Direct photon spectra for 200A GeV Au + Au collisions at RHIC and for 20–40% centrality bin [28] along with prompt (direct + fragmentation) and thermal (fluctuating (FIC) and smooth (SIC) initial density distributions) contributions. (b) v_2 with (solid) and without (dotted) the prompt photon contribution for smooth and fluctuating IC.

photon data for $200A$ GeV Au + Au collisions at RHIC and for 20–40% centrality bin [28] is compared with the prompt and thermal contributions (from smooth and fluctuating IC) in the upper panel of Fig. 8. We see from the figure that the prompt photons from the NLO pQCD calculation start to dominate the direct photon spectrum for $p_T > 4$ GeV/c. The direct (Compton + annihilation) and the fragmentation parts of the prompt photons are shown separately.[2] The fragmentation part dominates over the direct part for $p_T < 3.5$ GeV/c. We see that the thermal photons from fluctuating IC ($\sigma = 0.4$ fm) added together with the prompt photons explain the data really well in the region $p_T > 2$ GeV/c.

The elliptic flow is now calculated by adding the prompt contribution using the relation

$$v_2 = \frac{v_2^{th}\, dN^{th} + v_2^{pr}\, dN^{pr}}{dN^{th} + dN^{pr}} = \frac{v_2^{th}\, dN^{th}}{dN^{th} + dN^{pr}} \quad \text{as } v_2^{pr} \sim 0. \tag{9}$$

In Eq. (9) v_2^{th} and v_2^{pr} are the elliptic flow of thermal and prompt photons, respectively, and dN^{th} and dN^{pr} are the thermal and prompt yields. Addition of prompt contribution reduces the v_2 from the fluctuating IC by $\sim 25\%$ at $p_T = 2$ GeV/c and more than 50% at $p_T = 4$ GeV/c. The effect is larger for the v_2 from smooth IC than for the fluctuating IC, because fluctuations also increase the total thermal photon yield at high p_T.

D. Elliptic flow and spectra at LHC

The elliptic flow of thermal photons for $2.76A$ TeV Pb + Pb collisions at LHC and for 0–40% centrality bin is shown in upper panel of Fig. 9. Elliptic flow results from the fluctuating IC [v_2(PP) and v_2(RP)] are compared with the result obtained from a smooth initial state averaged IC. Similar to RHIC, fluctuations in the IC increase the elliptic flow significantly compared to a smooth IC in the region $p_T > 2$ GeV/c at LHC. Thermal photon v_2 from $200A$ GeV Au + Au collisions at RHIC using smooth IC is also shown for comparison. The elliptic flow at LHC is little larger than at RHIC for 0–40% centrality bin using smooth IC.

Our results for thermal photon elliptic flow from the fluctuating IC at LHC are compared with the ALICE preliminary direct photon v_2 data [17] in the lower panel of Fig. 9. As expected, the results from ideal hydrodynamic calculation are well below the experimental data for $p_T \leqslant 3.5$ GeV/c.

The thermal photon p_T spectra at LHC from the smooth and the fluctuating IC along with the ALICE preliminary direct photon data [38] are shown in the upper panel of Fig. 10. Prompt photons from NLO pQCD calculation along with the separate direct (Compton+annihilation) and fragmentation contributions are also shown for comparison. Similar to RHIC the direct photon spectrum is dominated by the prompt photons for $p_T > 4$ GeV/c at LHC. However, unlike at RHIC the fragmentation component at LHC is found to dominate over the direct component in the total prompt photon yield up to a very large p_T (~ 6 GeV/c). One can see that the thermal

---

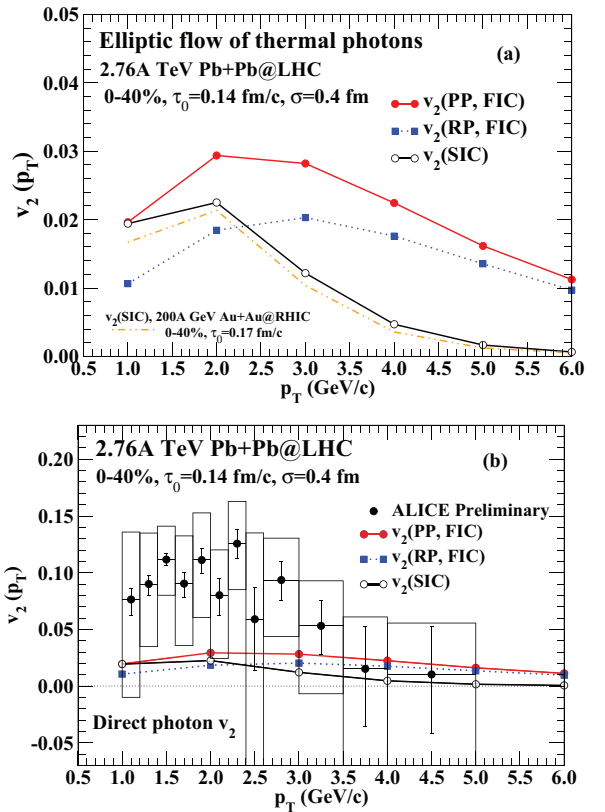[2]Understanding that such a separation conceptually depends on the scale choices.

FIG. 9. (Color online) (a) Elliptic flow of thermal photons for 0–40% central collisions of Pb nuclei at LHC. (b) Thermal photon elliptic flow and the ALICE preliminary direct photon v_2 data [17] at LHC.

photons from the fluctuating IC added together with the prompt photons explain the direct photon spectrum well in the region $p_T > 2.5$ GeV/c.

Inclusion of the prompt contribution reduces the photon v_2 at LHC (lower panel of Fig. 10) and the results are similar to the RHIC case.

IV. SUMMARY AND CONCLUSIONS

We have calculated the elliptic flow of thermal photons from an E-by-E ideal hydrodynamic model for Au + Au collisions at RHIC and Pb + Pb collisions at the LHC. In order to understand the physics processes underlying the photon v_2 better first we studied an individual event with different fluctuation size parameters. We saw that a smaller σ leads to larger momentum anisotropy and transverse flow velocity during the hydrodynamical evolution. However, at $p_T > 2.5$ GeV/c the photon elliptic flow with a small size parameter is an order of magnitude larger than with a large σ and this difference cannot be understood alone from the increase in the momentum anisotropy and the transverse flow velocity.

To understand the increase better, we studied the photon emission as a function of time in one single event. We see that with small size parameters the photon emission is enhanced much more at later times compared to the early times and thus
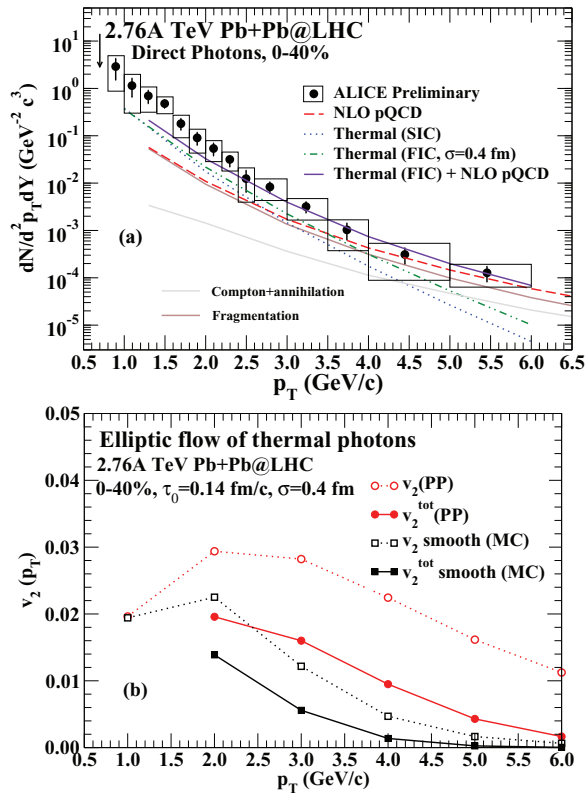
FIG. 10. (Color online) (a) Prompt (direct + fragmentation) and thermal (FIC and SIC) photons from $2.76A$ TeV Pb + Pb collisions at LHC for 0–40% centrality bin along with ALICE preliminary direct photon data [38]. (b) v_2 with and without the prompt photon contribution for smooth and fluctuating IC.

the average emission time gets larger for smaller σ due to the presence of hotspots in the IC. The elliptic flow is found to be larger for an E-by-E calculation at high p_T region compared to the smooth IC for $\sigma = 0.4$ fm. In addition, v_2(PP) with $\sigma = 1.0$ fm is found to be very similar to the result from smooth IC. At small p_T, the E-by-E calculations produce even a bit smaller photon elliptic flow than the smooth IC.

As for hadrons, the calculation of elliptic flow with respect to the participant plane gives a bit larger elliptic flow compared to the calculation with respect to reaction plane. However, there is a p_T dependence between the difference of the PP and RP results, which should be explored more in the future. Despite the fact that fluctuations may cause much larger v_2 for $p_T > 2.5$ GeV/c, the enhancement is still not sufficient to explain the PHENIX measurement even if we neglect all the other direct photon sources. We also calculated the elliptic flow of thermal photons at LHC from smooth and fluctuating IC and compare our results with the ALICE preliminary data. Similar to RHIC, fluctuations in the IC increase the elliptic flow significantly compared to a smooth profile for $p_T > 2$ GeV/c. Also at LHC our results are clearly below the measured elliptic flow by ALICE Collaboration [17].

We also calculated prompt photons from NLO pQCD at RHIC and LHC. Thermal photons from fluctuating IC along with prompt photons explain the PHENIX and the ALICE direct photon p_T spectrum well in the region $p_T > 2$ GeV/c and $p_T > 2.5$ GeV/c, respectively. The presence of the prompt photons in the direct photon spectrum reduces the elliptic flow [by adding more weight in the denominator as shown in Eq. (7)]. This reduction is 20–50% depending on the value of p_T for the fluctuating initial conditions and the reduction is even larger in the case of smooth initial conditions, because inclusion of density fluctuations also increases the total emitted photon yield.

[1] H. Holopainen, H. Niemi, and K. J. Eskola, Phys. Rev. C **83**, 034901 (2011).

[2] B. Schenke, P. Tribedy, and R. Venugopalan, Phys. Rev. Lett. **108**, 252301 (2012).

[3] J. S. Moreland, Z. Qiu, and U. W. Heinz, Nucl. Phys. A **904**, 815c (2013).

[4] C. E. Coleman-Smith, H. Petersen, and R. L. Wolpert, J. Phys. G **40**, 095103 (2013).

[5] Y. Hama, T. Kodama, and O. Socolowski, Braz. J. Phys. **35**, 24 (2005).

[6] R. Andrade, F. Grassi, Y. Hama, T. Kodama, and O. Socolowski, Phys. Rev. Lett. **97**, 202302 (2006); R. P. G. Andrade, F. Grassi, Y. Hama, T. Kodama, and W. L. Qian, ibid. **101**, 112301 (2008).

[7] B. Schenke, S. Jeon, and C. Gale, Phys. Rev. Lett. **106**, 042301 (2011).

[8] P. V. Ruuskanen, Nucl. Phys. A **544**, 169 (1992), and references therein; D. K. Srivastava, J. Phys. G **35**, 104026 (2008).

[9] R. Chatterjee, H. Holopainen, T. Renk, and K. J. Eskola, Phys. Rev. C **83**, 054908 (2011); J. Phys. G: Nucl. Part. Phys. **38**, 124136 (2011).

[10] R. Chatterjee, H. Holopainen, T. Renk, and K. J. Eskola, Phys. Rev. C **85**, 064910 (2012); arXiv:1207.6917.

[11] C. Adler et al. (STAR Collaboration), Phys. Rev. Lett. **87**, 182301 (2001); **89**, 132301 (2002); **90**, 032301 (2003); S. S. Adler et al. (PHENIX Collaboration), ibid. **91**, 182301 (2003).

[12] R. Chatterjee, E. S. Frodermann, U. W. Heinz, and D. K. Srivastava, Phys. Rev. Lett. **96**, 202302 (2006); R. Chatterjee and D. K. Srivastava, Phys. Rev. C **79**, 021901(R) (2009); U. W. Heinz, R. Chatterjee, E. S. Frodermann, C. Gale, and D. K. Srivastava, Nucl. Phys. A **783**, 379 (2007).

[13] H. Holopainen, S. S. Rasanen, and K. J. Eskola, Phys. Rev. C **84**, 064903 (2011).

[14] S. Turbide, C. Gale, E. Frodermann, and U. W. Heinz, Phys. Rev. C **77**, 024909 (2008).

[15] F. M. Liu, T. Hirano, K. Werner, and Y. Zhu, Phys. Rev. C **80**, 034905 (2009).

[16] A. Adare *et al.* (PHENIX Collaboration), Phys. Rev. Lett. **109**, 122302 (2012).

[17] D. Lohner for the ALICE Collaboration, arXiv:1212.3995.

[18] M. Dion, J.-F. Paquet, B. Schenke, C. Young, S. Jeon, and C. Gale, Phys. Rev. C **84**, 064901 (2011); C. Gale, arXiv:1208.2289 [hep-ph].

[19] S. T. Zalesak, J. Comput. Phys. **31**, 335 (1979).

[20] J. P. Boris and D. L. Book, J. Comput. Phys. **11**, 38 (1973).

[21] M. Laine and Y. Schroder, Phys. Rev. D **73**, 085009 (2006).

[22] K. J. Eskola, K. Kajantie, P. V. Ruuskanen, and K. Tuominen, Nucl. Phys. B **570**, 379 (2000).

[23] R. Paatelainen, K. J. Eskola, H. Holopainen, and K. Tuominen, Phys. Rev. C **87**, 044904 (2013).

[24] P. Arnold, G. D. Moore, and L. G. Yaffe, J. High Energy Phys. 12 (2001) 009.

[25] J. Ghiglieri, J. Hong, A. Kurkela, E. Lu, G. D. Moore, and D. Teaney, J. High Energy Phys. 05 (2013) 010.

[26] J. I. Kapusta, P. Lichard, and D. Seibert, Phys. Rev. D **44**, 2774 (1991); **47**, 4171(E) (1993).

[27] S. Turbide, R. Rapp, and C. Gale, Phys. Rev. C **69**, 014903 (2004).

[28] A. Adare *et al.* (PHENIX Collaboration), Phys. Rev. Lett. **104**, 132301 (2010).

[29] P. Aurenche, M. Fontannaz, J. P. Guillet, B. A. Kniehl, E. Pilon, and M. Werlen, Eur. Phys. J. C **9**, 107 (1999).

[30] F. Aversa, P. Chiappetta, M. Greco, and J. P. Guillet, Nucl. Phys. B **327**, 105 (1989).

[31] P. M. Nadolsky, H.-L. Lai, Q.-H. Cao, J. Huston, J. Pumplin, D. Stump, W.-K. Tung, and C.-P. Yuan, Phys. Rev. D **78**, 013004 (2008).

[32] I. Helenius, K. J. Eskola, H. Honkanen, and C. A. Salgado, J. High Energy Phys. 07 (2012) 073.

[33] L. Bourhis, M. Fontannaz, and J. P. Guillet, Eur. Phys. J. C **2**, 529 (1998).

[34] S. Afanasiev *et al.* (PHENIX Collaboration), Phys. Rev. Lett. **109**, 152302 (2012).

[35] S. Chatrchyan *et al.* (CMS Collaboration), Phys. Lett. B **710**, 256 (2012).

[36] I. Helenius, K. J. Eskola, and H. Paukkunen, J. High Energy Phys. 05 (2013) 030.

[37] T. Renk, Int. J. Mod. Phys. E **20**, 1594 (2011).

[38] M. Wilde for the ALICE Collaboration, arXiv:1210.5958.